JOURNAL OF GEOPHYSICAL RESEARCH, VOL. 101, NO. A9, PAGES 19,921–19,936, SEPTEMBER 1, 1996

Electromagnetic characteristics of the high-latitude ionosphere during the various phases of magnetic substorms

Y. I. Feldstein, L. I. Gromova, and A. E. Levitin

IZMIRAN, Troitsk, Moscow Region, Russia

L. G. Blomberg, G. T. Marklund, and P.-A. Lindqvist

Alfvén Laboratory, Royal Institute of Technology, Stockholm, Sweden

Abstract. Model calculations of the electrodynamics of the high-latitude ionosphere are compared to measurements made by the Viking satellite during July-August 1986. The model calculations are based on the IZMEM procedure, where the electric field and currents in the ionosphere are given as functions of the interplanetary magnetic field. The events chosen correspond to the growth, the expansion, and the recovery phases of substorms. During the growth and expansion phases the correlation between the model results and the satellite data is rather good. During recovery phase the correlation is not as good. The correlation between modeled and observed quantities suggest that during growth and expansion phase the magnetosphere is mainly directly driven by the solar wind, whereas during recovery phase it is mainly driven by internal processes, i.e., loading-unloading. Best fit is obtained when averaging the measured quantities over a few minutes, which means adjusting the spatial resolution of the measurements to the resolution of the model. Different time delays between the interplanetary magnetic field observations and those of Viking were examined. Best agreement was obtained, not surprisingly, for time delays corresponding to the estimated information transit time from the solar wind spacecraft to the ionosphere.

Introduction

Observations of various phenomena in the polar caps are relatively sparse, and therefore our knowledge of the global electrodynamics in these regions is generally based on inferences drawn from statistical analysis of large data sets or from event studies.

In the geospace environment modeling (GEM) program, two models are considered for synthesis of sparse high-latitude data [*Lotko*, 1993]. Both models allow the computation of nearly instantaneous snapshots of electric field and potential distribution in the entire auroral region. The assimilative mapping of ionospheric electrodynamics (AMIE) model is used for calculation of high-latitude electric fields and currents from sets of localized observational data [*Richmond and Kamide*, 1988; *Richmond et al.*, 1988; *Richmond*, 1992]. A similar model has also been used by *Marklund et al.* [1988]. See also *Marklund and Blomberg* [1991] and *Blomberg and Marklund* [1993]. The Institute of Terrestrial Magnetism Electrodynamical Model (IZMEM) is another model for calculating the same parameters, but the input data are the interplanetary magnetic field (IMF) magnitude and direction [*Levitin et al.*, 1984; *Feldstein and Levitin*, 1986; *Papitashvili et al.*, 1994]. The influence of the IMF on the upper atmosphere electrodynamics is crucial also in the models of *Friis-Christensen et al.* [1985] and *Mishin* [1990]. The latter two models are used by their respective authors only, whereas the IZMEM model is publicly available through the World Data Center A for Rockets and Satellites [*Bilitza*, 1990].

The IZMEM model is here used to determine the global convection pattern and its temporal evolution during a number of passes of the Swedish satellite Viking over the northern high-latitude region. The model electric field is compared to the satellite observations along the trajectory, and the global convection pattern and its temporal evolution is estimated in the entire high-latitude region. The sensitivity to averaging of the correlation between the modeled and measured values is discussed. The averaging interval selected influences the sensitivity of the correlation to changes in the model, and it is of interest to determine to what extent the correlation coefficient is dependent on the correct timing of the changes between gross features of the convection system during the period studied.

Paper number 96JA00514.
0148-0227/96/96JA-00514$09.00

There is today a consensus that there are two processes responsible for the solar wind energy input to the magnetosphere during substorms. These are direct driving and loading-unloading processes. Some fraction of the energy input is directly dissipated in the ionosphere by Joule heating and particle precipitation related to enhanced convection and enhanced ionospheric currents. This power dissipation is directly correlated with the solar wind parameters and is thus a driven process [*Akasofu*, 1981]. The remaining part of the power transfered into the magnetosphere is stored temporarily in the Earth's magnetosphere and subsequently released at substorm breakup. The latter is known as loading-unloading process [*Baker et al.*, 1984, 1993].

The delay time between a change in the IMF and the related effects in the ionosphere is different for the two processes. For the directly driven process it is 10-20 min due to the inductance of the magnetosphere-ionosphere system. For the loading-unloading process it is typically 40-60 min. Which one of these processes dominates remains an open question.

Additional light may be shed on this problem by comparing the IZMEM model electric fields with those observed by Viking during different phases of substorms. The IZMEM model assumes a linear dependence of the ionospheric electric field on the IMF (i.e., a direct driving). Therefore the correlation obtained between the measured and the modeled electric fields may be used as an indicator of which process is dominating.

The second section contains brief descriptions of the model calculations and of the Viking electric field measurements. Results of the model calculations projected on the Viking trajectory are compared with observational data in section 3. The last sections contain a discussion of the results and conclusions of this study.

Model and Experiment Description

The large-scale distribution of convection above the ionosphere is conveniently represented by the electrostatic potential Φ. Here the IZMEM model is used where Φ is obtained by numerical integration of a second-order partial differential equation with a known current function ψ [*Faermark*, 1977].

For the case of a nonuniform ionospheric conductivity, this equation is

$$-\left[\frac{\partial}{\partial\theta}\left(\sin\theta\Sigma_H\frac{\partial\Phi}{\partial\theta}\right)\right]+\frac{1}{\sin\theta}\frac{\partial}{\partial\lambda}\left(\Sigma_H\frac{\partial\Phi}{\partial\lambda}\right)+\left[\frac{\partial}{\partial\theta}\left(\Sigma_P\frac{\partial\Phi}{\partial\lambda}\right)-\frac{\partial}{\partial\lambda}\left(\Sigma_P\frac{\partial\Phi}{\partial\theta}\right)\right]=\frac{\partial}{\partial\theta}\left(\sin\theta\frac{\partial\psi}{\partial\theta}\right)+\frac{1}{\sin\theta}\frac{\partial^2\psi}{\partial\lambda^2} \quad (1)$$

with the boundary condition

$$\Phi(\theta=34^\circ)=0 \quad (2)$$

Here θ and λ are the colatitude and longitude, respectively, in spherical coordinates. Σ_H and Σ_P are the height-integrated Hall and Pedersen conductivities. Σ_H and Σ_P are composed of the conductivities resulting from both solar UV radiation and particle precipitation. The contribution of particle precipitation is based on the statistical conductivity model of *Wallis and Budzinsky* [1981], and the contribution of solar UV conductivity is based on the model of *Robinson and Vondrak* [1984].

The model current is unambiguously related to the variation of the horizontal magnetic field at the Earth's surface and was estimated from the spatio-temporal distribution of geomagnetic field variations measured by the world-wide ground-based magnetometer network. The definition of the model current in the IZMEM model is similar to that in the model by *Kamide et al.* [1981].

The dependence of the magnetic variations at high latitudes on the magnetic field and plasma parameters of the solar wind may be obtained by regression methods. According to *Levitin et al.* [1982], the horizontal and vertical components of the field variation at the Earth's surface in the $\theta \leq 30^\circ$ colatitude region may be expressed as

$$H_E^i = K_i^{B_y}B_y+K_i^{B_z}B_z+K_i^{B_x}B_x+K_i^{nv^2}nv^2+K_i^{v^2}v^2+H_0^i \quad (3)$$

where B_y, B_z, and B_x are the IMF components and v and n are the solar wind velocity and density. This series is assumed to be sufficient for describing the relation between quasistationary variations in the Earth's magnetosphere and variations in the interplanetary medium. The addition of new terms does not improve the agreement between the observed and the model values of H_E^i. The coefficients K_i are found by least squares analysis, as described by *Levitin et al.* [1982]. Each of the terms in the series represents the geomagnetic response to a certain parameter of the interplanetary medium, while the residual term H_0^i represents the extrapolation of the midlatitude S_q current system to high latitudes.

The coefficients $K_i^{B_x}$ are much smaller than $K_i^{B_y}$ and $K_i^{B_z}$, while the terms depending on n and v may be combined with H_{0i} to a single constant $H_0 = K_i^{nv^2}nv^2+K_i^{v^2}v^2+H_0^i$, which characterizes the average conditions in the solar wind ($n = 4$ cm^{-3} and $v = 500$ km/s [cf. *Levitin et al.*, 1982]). Thus for average solar wind plasma parameters, (3) may be simplified to

$$H_E^i = K_i^{B_y}B_y + K_i^{B_z}B_z + H_0. \quad (4)$$

Equation (3) must be used for extreme values of n and v.

Spatial distributions of the coefficients $K_i^{B_y}$, $K_i^{B_z}$, and H_0 are an integral part of the model of *Levitin et al.* [1984]. This model also contains values of the potentials Φ_y^m, Φ_z^m, and Φ_0^m obtained by solving (1) with the boundary condition (2), where the model current is determined by the corresponding sets of coefficients $K_i^{B_y}$, $K_i^{B_z}$, and H_0.

The potential Φ_m at the point (IL, MLT) is represented by

$$\Phi^m(IL, MLT, B_y, B_z) = \Phi_y^m(IL, MLT)B_y$$

$$+\Phi_z^m(IL, MLT)B_z + \Phi_0^m(IL, MLT) \quad (5)$$

where B_y and B_z are the values of the IMF for the time when Φ_m is determined. For $B_z \geq 0$ and $B_z < 0$ conditions the model of *Wallis and Budzinski* [1981] is used at $K_P < 3$ and $K_P > 3$, respectively. $\Phi_y^m(IL, MLT)$, $\Phi_z^m(IL, MLT)$ and $\Phi_0^m(IL, MLT)$ are basis functions for the electrostatic potential (and hence the convection) in the high-latitude ionosphere. As a result, one can obtain the distribution of $\Phi^m(IL, MLT, B_y, B_z)$ for any orientation of the IMF.

The representation of the ionospheric convection pattern by the sum of elementary contributions Φ_y^m, Φ_z^m, and Φ_0^m according to *Levitin et al.* [1984] is in agreement with the three types of magnetospheric convection cells suggested by *Burch et al. [1985]* and by *Reiff and Burch* [1985]. Their merging cells are equivalent to Φ_z^m for $B_z < 0$, the viscous cells are equivalent to Φ_0^m for $B_z = B_y = 0$, and the lobe cells correspond to Φ_y^m and Φ_z^m for $B_z > 0$. Since $\mathbf{E} = -\nabla\Phi$ (if $\nabla \times \mathbf{E} = 0$, which is assumed here), ∇ is a linear differential operator, and B_y and B_z have no spatial dependence (at ionospheric altitude), an expression exactly analogous to (5) exists for the modeled electric field $\mathbf{E}^m = -\nabla\Phi^m$.

The electric field experiment on Viking consisted of six spherical probes extended on wire booms from the satellite [e.g., *Block et al.*, 1987]. Four of these booms were 40 m long and located in the plane perpendicular to the spin axis. These probes provide information about the two spin plane components of the electric field, one often being nearly parallel to the magnetic field (the component E_1) and the other being perpendicular to **B** and directed nearly opposite to the satellite's velocity vector (the component E_2). The latter, which is used in this study, is typically the dominant electric field component perpendicular to **B**.

The angle between axis 2 and the satellite velocity vector varied in the range from $\sim 160°$ to $\sim 175°$. Information about the third electric field component is unfortunately missing since one of the probes was damaged early in the mission. For more information on the electric field instrument, see *Block et al.* [1987].

Convection and Electric Field Variations Over the Ionosphere During the Different Phases of Magnetospheric Substorms

Five Viking passes were selected for electric field modeling. UV images from Viking of the global auroral distribution are available for all events [*Cogger and Mur-*

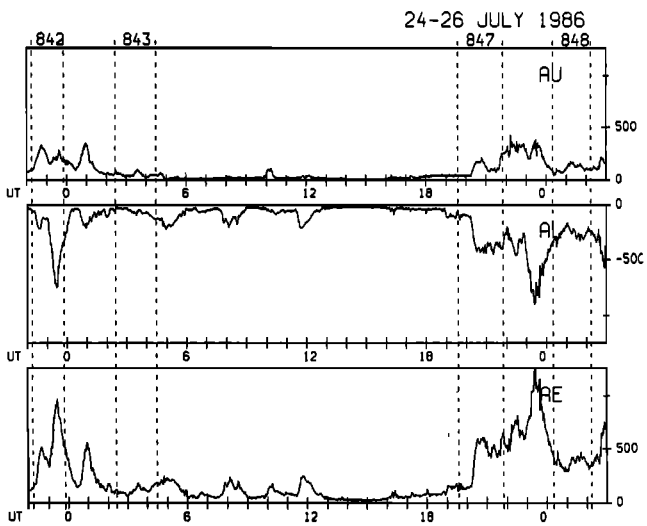

Figure 1. The perpendicular component of the electric field measured by Viking, E_2, the interplanetary magnetic field (IMF) z and y components, and AU, AL, and AE, respectively, for the four events occurring July 24-26, 1986.

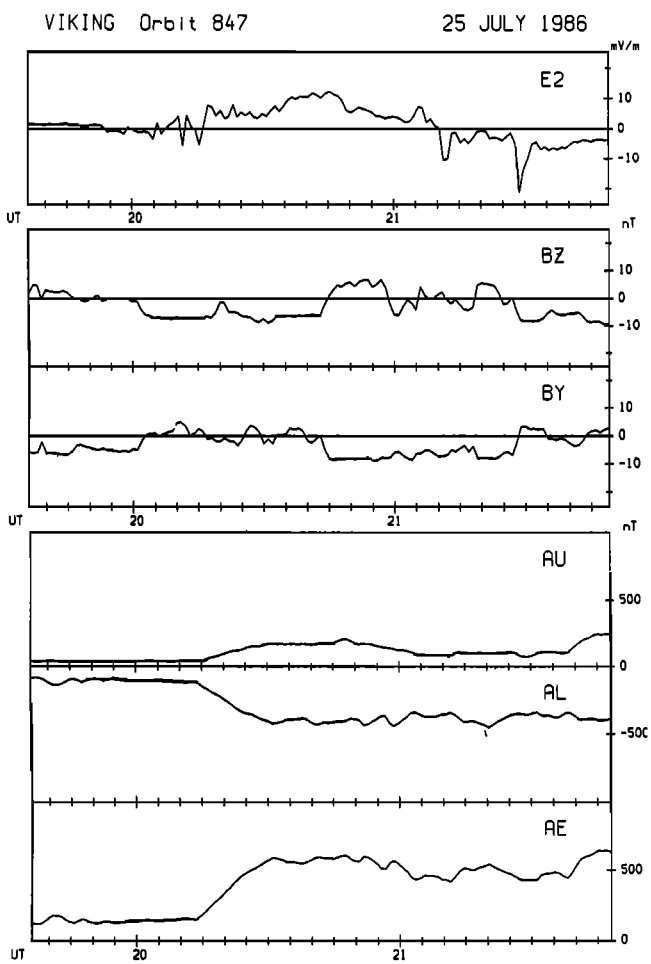

Figure 2. One-minute averages of, E_2, IMF B_z and B_y, and AU, AL, and AE for Viking pass 847 over the high-latitude region on July 25, 1986. The IMP 8 spacecraft position is (6.1, 32.5, -5.1) R_E.

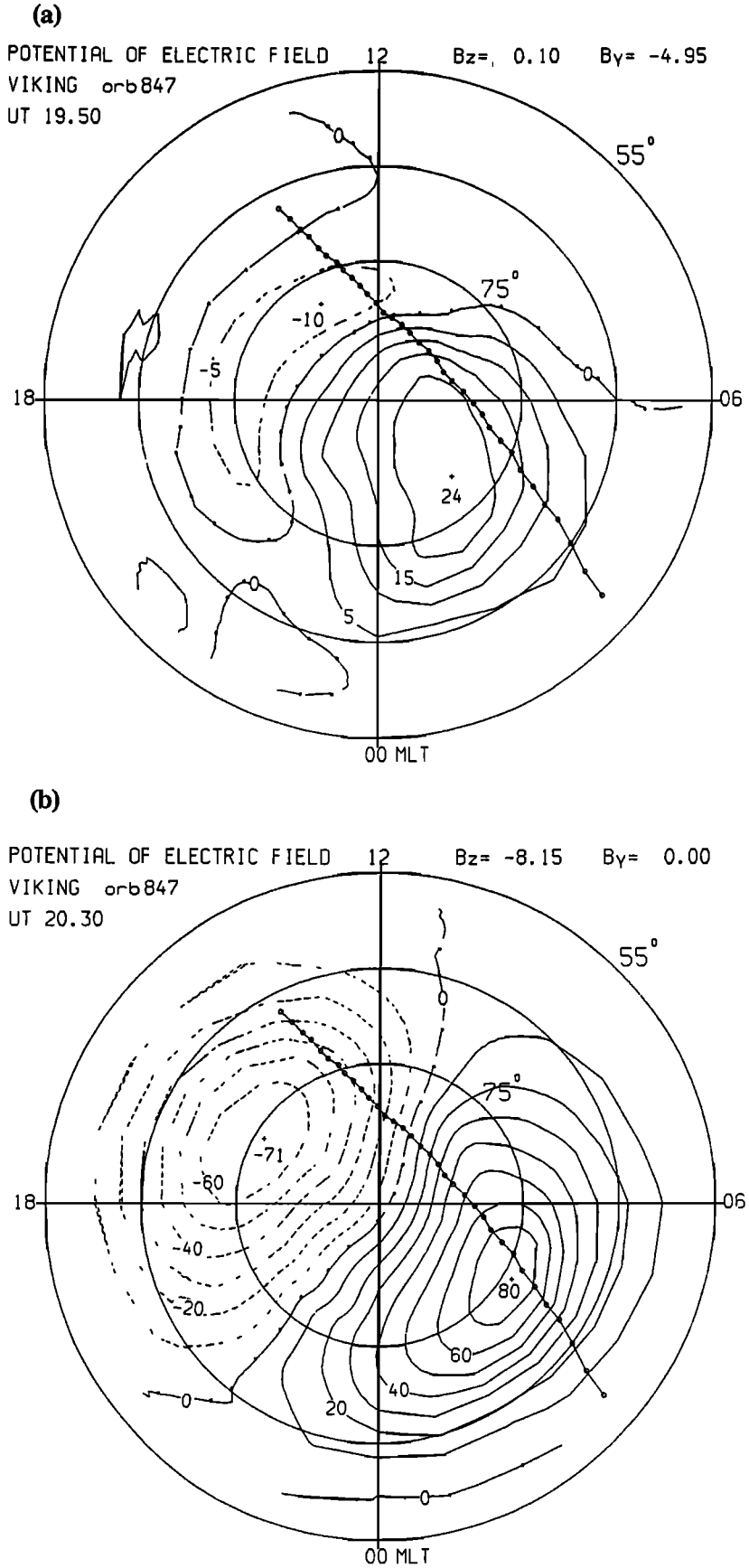

Figure 3. The convection patterns at (a) 1950 UT and (b) 2030 UT on July 25, 1986 for the IMF component values of $B_z = 0.1$ nT and $B_y = -4.95$ nT; $B_z = -8.15$ nT and $B_y = 0.0$ nT, respectively.

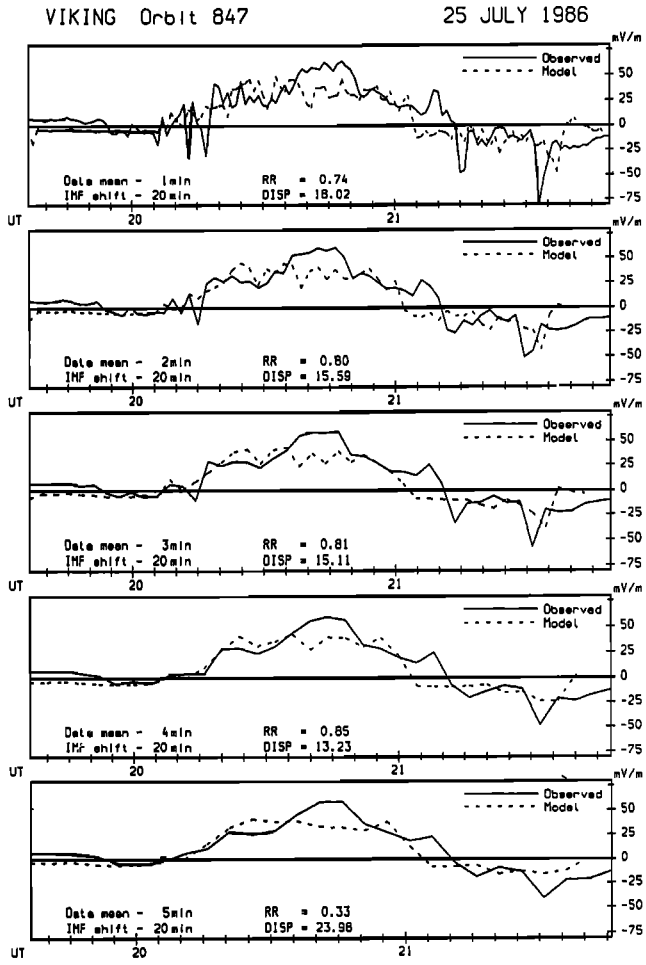

Figure 4. Comparison of the horizontal electric field components measured by Viking and mapped along dipole magnetic field lines to 100 km altitude (E_2 solid line) and calculated (E_2^m dotted line) with various averaging time step for the IMF and E_2 values but with a constant IMF time shift $\Delta T = 20$ min. From top to the bottom time-averaging values of 1, 2, 3, 4, and 5 min are presented. The correlation coefficient and mean square deviations values are also presented.

phree, 1990]. Figure 1 shows the perpendicular electric field measured by Viking and mapped to 100 km altitude, the IMF z and y components, and the electrojet indices which indicate that Viking pass 842 on July 24 occurred during the expansion phase, passes 843 and 848 on July 25 and 26 occurred during the recovery phase and pass 847 occurred during the growth phase and the subsequent transition to the expansion phase (vertical lines mark time intervals of each pass).

The values of E_2^m were calculated by averaging the IMF values over between 1 and 15 min. The delay time relative to the IMF measurements was varied from 10 to 25 min. The values of E_2^m thus obtained were compared to measured values of the horizontal component E_2 of the electric field along the Viking trajectory. The values of E_2 are spin-averaged data (20 s) which have been further averaged over the same time as E_2^m. When correlating E_2^m and E_2, E_2 was mapped from the satellite altitude down to 100 km altitude, assuming no parallel potential drop in between. This altitude corresponds to the ionospheric region where the main current flows. The correlation coefficient and the dispersion between E_2^m and E_2 were calculated for each of the five examples presented below.

Growth Phase

Viking pass 847 on 25 July 1986 1940-2145 UT occurred during substorm growth phase and the beginning of expansion phase. Figure 2 shows the transverse electric field observed by Viking, the IMF components B_z and B_y, and the magnetic activity indices AU, AL and AE. Magnetic activity in the auroral zone began 15 min after the southward turning of B_z because of the simultaneous increase of both the westward and eastward electrojets.

As the IMF evolves with time so does the large-scale ionospheric convection pattern. Figure 3 presents the modeled electrostatic potential at 1950 and 2030 UT. At 1950 UT the dawn convection cell is dominating, whereas at 2030 UT the dawn and dusk cells are roughly equal. A comparison was made between the measured transverse electric field mapped to 100 km altitude and the corresponding component of the modeled field along the satellite trajectory. The result is shown in Figure 4 where the solid curves are the observed field, and the dashed ones are the model field. The different panels represent different time averaging intervals ranging from 1 min (top) to 5 min (bottom). The IMF time delay (ΔT) is 20 min in all cases. Maximum correlation (correlation coefficient $RR = 0.85$, and mean square deviation (dispersion) $DISP = 13$ mV/m) between observations and modeling results is obtained for an averaging interval of 4 minutes. Thus, for this event there is a rather good correlation between the modeled electric field and the observations (along the satellite trajectory). This implies that direct driving dominates as the energy transfer mechanism between the solar wind and the magnetosphere during the growth and expansion phases of substorms. We have also checked different delay times of the IMF data. Best fit was obtained for $\Delta T = 20$ minutes. The estimated time needed for the IMF to propagate from IMP 8 to the magnetopause is 14 min assuming that the "IMF wave front" is parallel to the direction of propagation, and 3 min assuming that the IMF propagates radially away from the Sun. Hence intramagnetospheric processes introduce a time delay of between 6 and 17 min.

Expansion Phase

Viking pass 842, July 24, 1986, 2215-2350 UT occurred during the expansion phase of a substorm. Figure 5 shows the transverse electric field observed by Viking, the IMF components B_z and B_y, and the magnetic activity indices AU, AL, and AE (the format is equivalent to that of Figure 2). IMF B_z is strongly

southward, almost 20 nT, until 2310 UT when it changes abruptly to being strongly northward. During the course of the pass the modeled ionospheric convection pattern changes from a two-cell pattern with the flow lines converging at the center of the polar cap at 2225 UT, to a two-cell system with the flow lines converging at the dawn side at 2305 UT. The asymmetry is introduced because of a substantial change of IMF B_y. Later, at 2320 UT the convection pattern is practically a single-cell system centered around the magnetic pole. Using the IMF data as are gives a modeled polar cap potential drop exceeding 300 kV. This unrealistically high value is a result of the linear dependence in the model of the potential on the IMF. The solar wind - magnetosphere interaction is known to saturate when the southward IMF B_z exceeds 10 nT [*Reiff and Luhmann*, 1986; *Dremuhina et al.*, 1990] To account for this, we have used the value 10 nT as input to the model whenever B_z exceeds 10 nT. Figure 6a shows the convection pattern modeled at 2305 UT taking this saturation effect into account. The polar cap voltage is 181 kV, still high. The model electric field vectors along the Viking trajectory are shown in Figure 6b. The field magnitude is high on the dayside but decreases as the satellite moves toward the nightside. This is not only a result of the spatial variation of the convection pattern but it also reflects the northward turning of the IMF at 2310 UT, about half ways through the Viking pass.

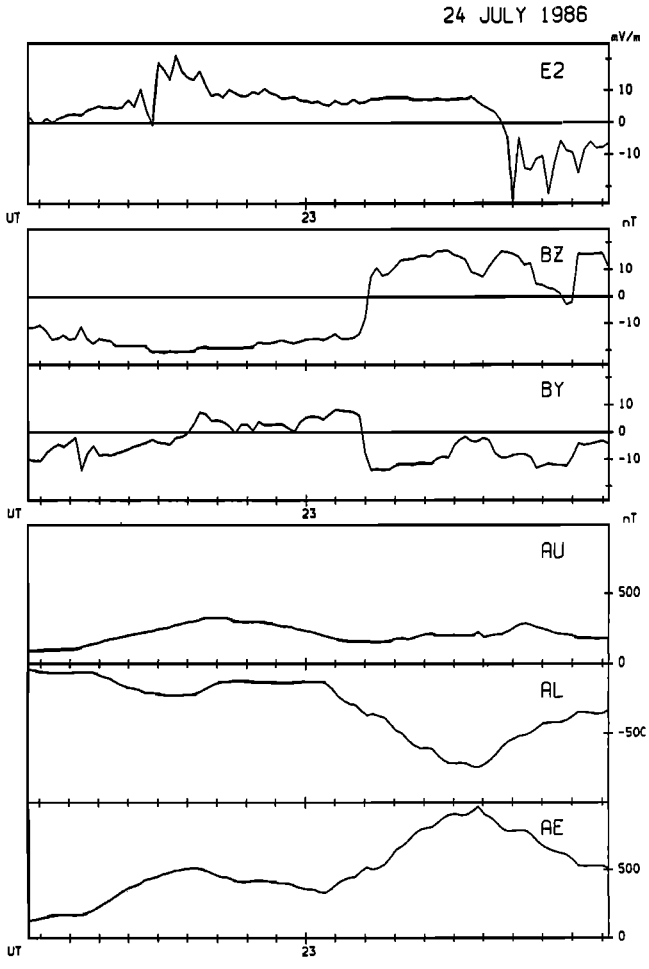

Figure 5. Similar to Figure 2, but for Viking pass 842. The IMP 8 location was (18.6, 27.5, -10.9) R_E.

The agreement between modeled and measured electric field depends critically on the IMF delay time as well as on the averaging interval chosen. Figure 7 shows the transverse electric field measured by Viking and mapped to 100 km altitude together with the modeled field along the trajectory. The IMF delay is 25 min in all panels, but the averaging interval changes from 1 min (top) to 5 min (bottom). The correlation is practically the same ($r = 0.9$) for averaging intervals of 3, 4, and 5 min. The overall agreement is good. The only significant discrepancy occurs toward the end of the pass when Viking enters the morning sector auroral oval.

The effect of different IMF delay times on the modeling results is shown in Figure 8. The delay increases from 15 min (top) to 30 min (bottom) in steps of 5 min. The averaging interval is 5 min in all panels. Best fit is obtained for $\Delta T = 25$ min, for which the correlation maximizes ($r = 0.9$) and the dispersion minimizes ($d = 20.8$ mV/m). In addition, it is clearly seen that the peaks and reversals of the electric field are well co-located for this particular choice of ΔT.

The time delay of IMF propagation from IMP 8 to the magnetopause is estimated to be 20 min, allowing for the IMF direction, and 7 min assuming radial expansion. Thus the intramagnetospheric delay was between 5 and 18 min for this event.

Recovery Phase

Viking pass 843, July 25, 1986, 0225-0415 UT occurred during substorm recovery. In Figure 9 are shown the transverse electric field observed by Viking, the IMF components B_z and B_y, and the magnetic activity indices AU, AL, and AE (the format is equivalent to that of Figure 2). The IMF is significantly weaker than in the previous cases, the electrojets have faded, but the electric field remains rather strong. All this is characteristic for the recovery phase. The modeled high-latitude convection pattern (Figure 10a) is basically of a single-cell type with anticlockwise plasma circulation in the cell. The flow lines are somewhat squeezed together on the dayside. Figure 10b shows the model electric field vectors along the Viking trajectory for a ΔT of 20 min.

Regardless of the averaging interval, the correlation is low ($r < 0.58$), i.e., significantly lower than for the growth and expansion phase events discussed above. This implies that the directly driven process does not dominate during recovery phase in contrast to growth and expansion phase. Rather, during recovery phase the magnetosphere is driven, at least to a significant part, by a loading-unloading process. The maximum (i.e., least bad) correlation is obtained for $\Delta T = 20$ min. IMF propagation time from IMP 8 to the magne-

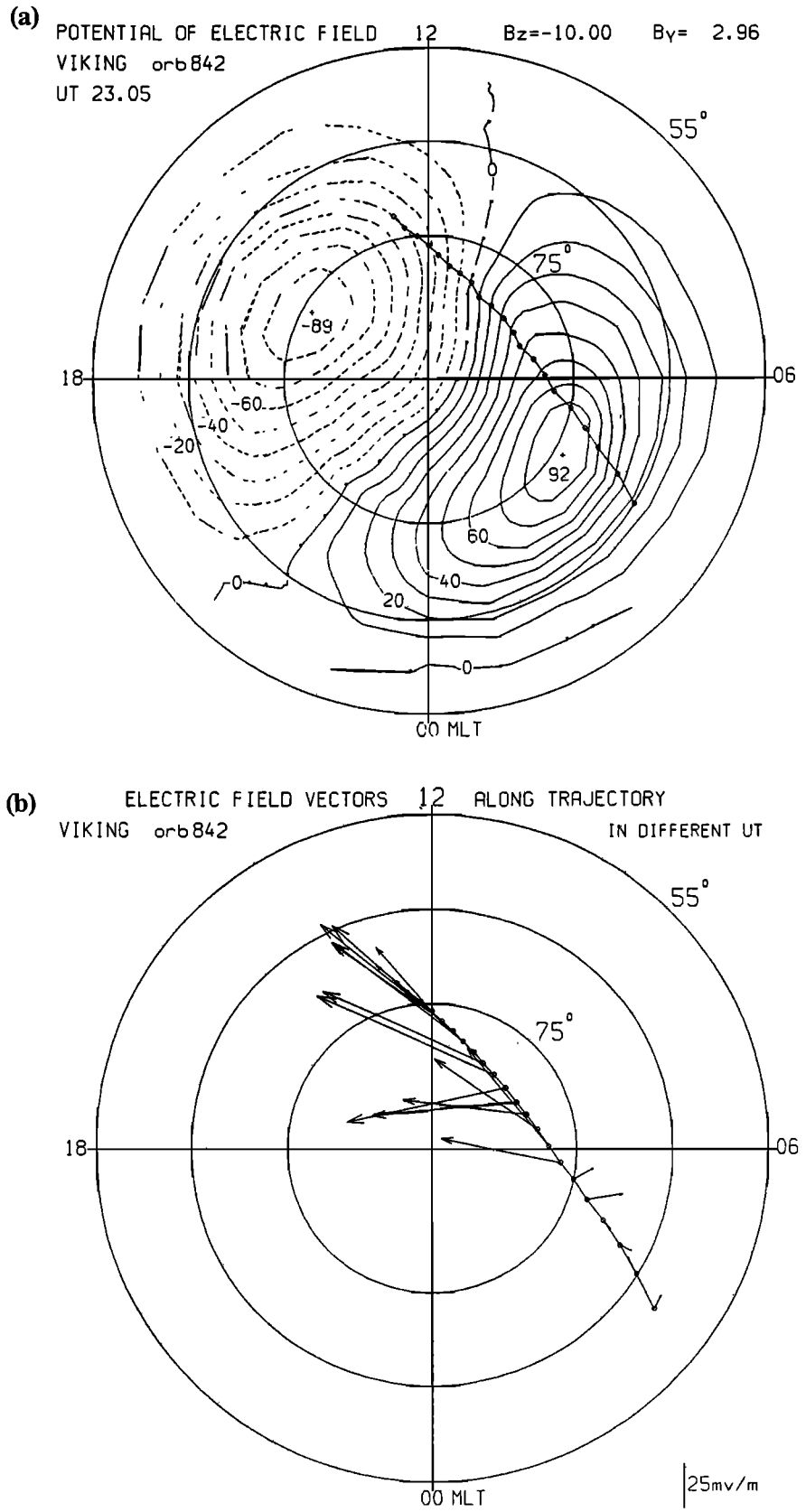

Figure 6. (a) The northern hemisphere high-latitude convection pattern at 2305 UT on July 24, 1986, allowing for the IMF B_z component intensity restriction (the saturation effect). Extrema of the potential values are indicated in the foci. Solid lines correspond to anticlockwise convection, and dotted lines to clockwise convection. The polygonal line is the satellite track, the dots correspond to the satellite location every 5 min between 2215 and 2350 UT. (b) Electric field vectors E^m along the satellite track for each 5-min interval using IMF shift $\Delta T = 25$ min.

topause is estimated at 17 min accounting for the IMF direction and 5.5 min without accounting for it. Hence the intramagnetospheric delay was between 7 and 14.5 min in this event.

Another example of recovery phase is Viking pass 848, July 26, 1986, 0020-0210 UT. Figure 11 presents the measured electric field, the IMF data, and the electrojet indices. The electric field is rather strong throughout the pass while the IMF and electrojets are rather weak, again typical of recovery phase. The modeled large-scale convection pattern is of a two-cell type with antisolar plasma flow across the central part of the polar cap.

The measured and the modeled electric fields were compared along the Viking trajectory using different

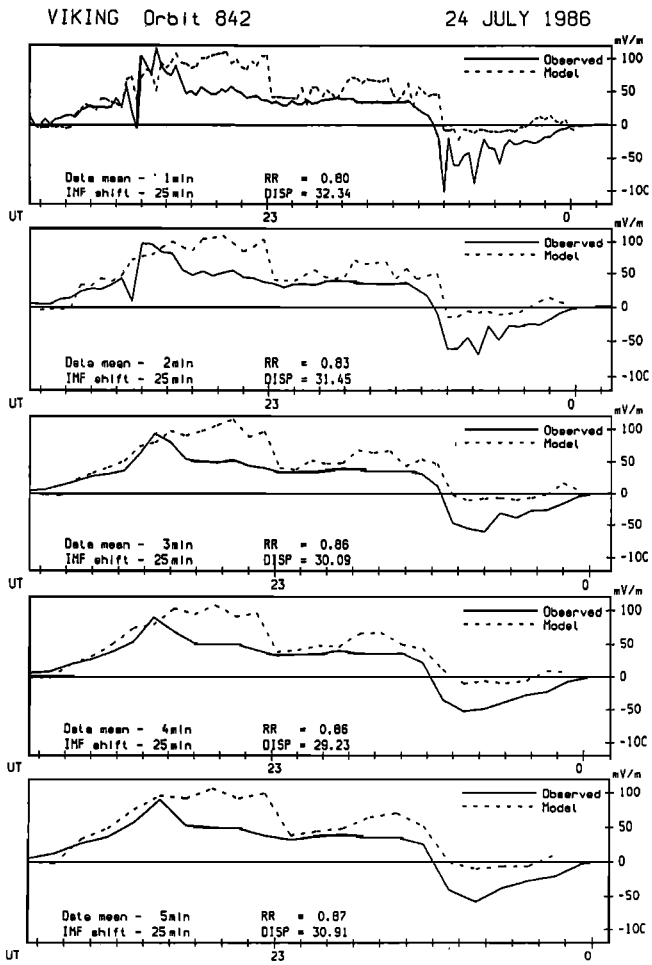

Figure 7. Comparison of the horizontal electric field components measured by Viking and mapped along dipole magnetic field lines to 100 km altitude (E_2 solid line) and calculated allowing for the saturation effect (E_2^m dotted line) with various averaging time intervals for IMF and E_2 but with a constant IMF time shift ΔT = 25 min. From top to bottom time averaging intervals of 1, 2, 3, 4, and 5 min are presented. The correlation coefficient and mean square deviations values are also presented.

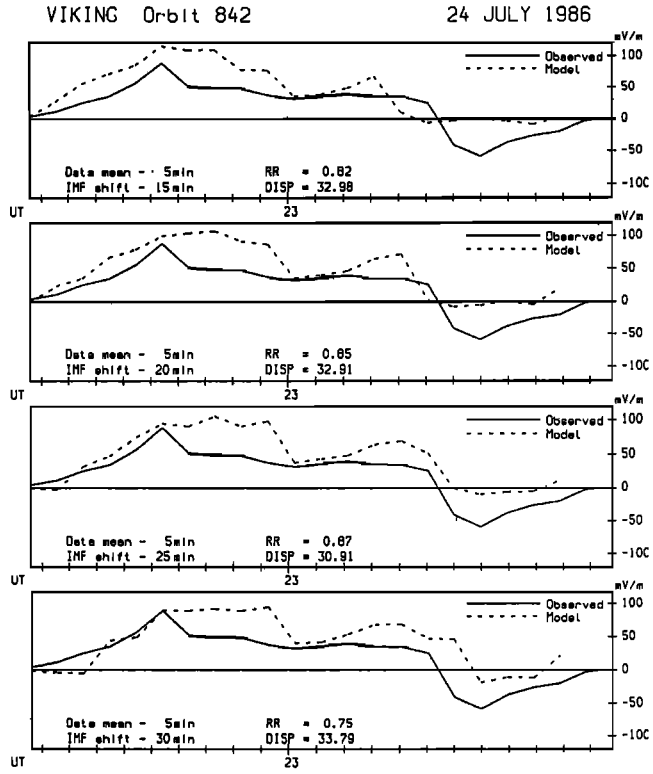

Figure 8. Comparison of E_2 and E_2^m for various values of the IMF time shift ΔT relative to E_2 using a constant time averaging interval of 5 min.

IMF delay (or lead) times and also different averaging intervals. Best correlation was found for a 5-min averaging, consistent with the events discussed above. Figure 12 compares the measured and modeled fields for different ΔT. In the top panel $\Delta T = -5$ min, i.e., the ionospheric convection leads the IMF variations by 5 min. In the lower three panels ΔT equals, 0, 5, and 10 min, respectively. The best correlation is obtained for a zero or slightly negative delay time. In all cases there is an overall agreement of the directions of the measured and modelel fields, but the magnitude of the model field is consistently smaller than the measured one.

The fact that the best correlation was obtained for a nonpositive delay time demonstrates two things. First, that it is crucial in general that the delay time be chosen properly. Second, that in this particular case, substorm recovery phase, the directly driven assumption is not viable but rather a loading-unloading process is likely.

Growth Phase Following a Transpolar Arc

Parameters of the interplanetary medium and magnetic activity during the substorm on August 3, 1986, have been discussed by *Feldstein et al.* [1995]. At the beginning of Viking pass 896, 1710-1920 UT, both B_z and B_y were positive ($B_z \sim 9$ nT, $B_y \sim 8$ nT). After crossing the zero level at 1750-1802 UT, both components were negative at the end of the pass. A polar arc existed in the polar cap of the southern hemisphere

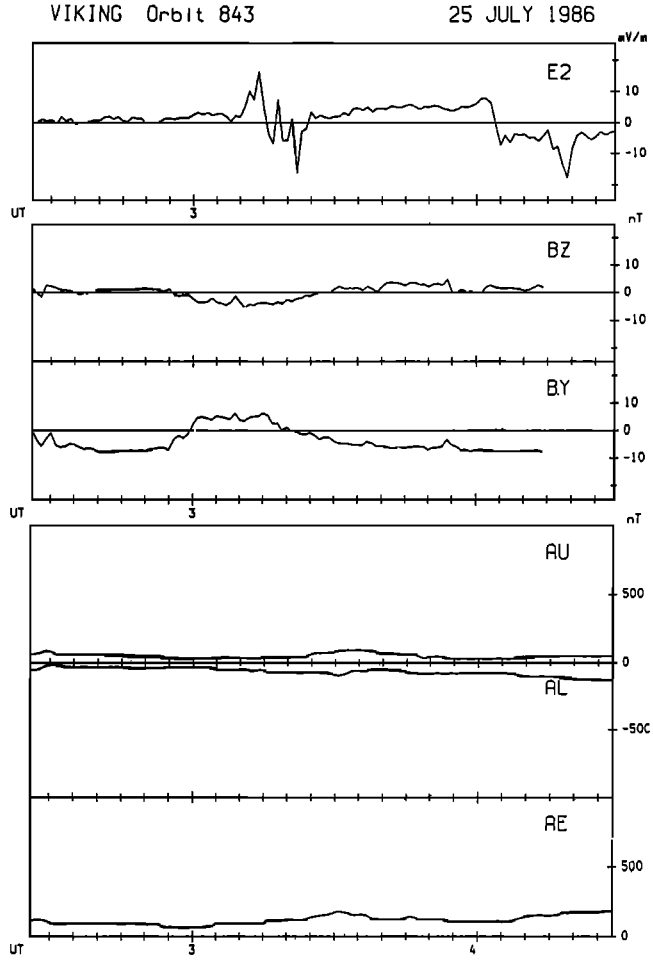

Figure 9. Similar to Figure 2 but for Viking pass 843 over the high-latitude region on July 25, 1986. The IMP 8 spacecraft is at (17.3, 28.3, −10.3) R_E.

prior to the Viking pass [*Vorobjev et al.*, 1995], which was seen after 1800 UT simultaneously in both hemispheres [*Craven et al.*, 1991]. After B_z turns southward, the polar arc rapidly moves across the polar cap towards dawn (dusk) in the northern (southern) hemisphere. Thus the event under consideration is a rare case of a persistent θ aurora during southward IMF.

From 1500 to 1800 UT the magnitude of magnetic disturbances in the auroral zone is small and decreasing for northward IMF. At 1800 UT, the *AU* and *AL* indices start to increase, reflecting a smooth increase of both the eastward and westward electrojets. A study of the horizontal (northward) magnetic field component along the meridional chain of magnetic observatories traversing the auroral zone in the midnight sector shows that the substorm expansion phase started at 2015 UT. Before this time the decrease of the X component is maximum at 70°-72° invariant latitude, with essentially no disturbances at IL ~ 67°. These characteristics are typical for the growth phase of a magnetospheric substorm [*McPherron*, 1970; *Feldstein*, 1974]. The expansion phase at 2015 UT is accompanied by an increase in the *AL* index, stemming from the corresponding decrease in the horizontal component at IL~ 67°. Thus the Viking pass began during relatively quiet magnetospheric conditions and finished during the substorm growth phase.

During the initial part of the pass the whole polar cap is covered by a vortex with clockwise plasma convection (Figure 13). Such a one-cell convection system is similar to that described earlier by *Feldstein et al.* [1984], *Burch et al.* [1985], and *Friis-Christensen et al.* [1985] for the same IMF B_y polarity. Starting at the substorm growth phase, a two-cell convection system is established, which means that the model convection distribution and hence the electric fields substantially change during the satellite pass. This means that in the model calculation of ionospheric parameters along the satellite track temporal variations in the IMF must be taken into account.

Figure 14 shows E_2^m and E_2 for different values of the IMF delay time ΔT, with an averaging interval of 5 min. It is worth mentioning the improvement in the correlation up to RR=0.90 as ΔT increases from 10 to 20 min. Even the sharp decrease of E_2 at 1805 UT is reflected in the model output for $\Delta T = 20$ min. RR decreases and DISP increases rapidly as ΔT increases beyond 20 min. It appears that for this Viking pass on August 3, 1986, which occurs during the substorm growth phase, the model reasonably well describes the distribution of and variations in the observed electric field. This agreement between E_2^m and E_2 suggests that the model can be used to describe the temporal evolution of the electrostatic potential distribution (convection pattern) and the electric field over the entire high-latitude region.

The high correlation between the observed electric fields and those predicted by the model indicates that the magnetosphere is closely controlled by the IMF during the substorm growth phase. Apparently, the magnetosphere is at this stage of the substorm directly driven by the solar wind. Processes within the magnetosphere connected with the unloading of magnetic energy stored in the magnetospheric tail have only a secondary role.

Small-scale variations of the electric field in the vicinity of a θ aurora lies beyond the possibilities of the model. In this event, this is seen in the time interval 1837-1906 UT, marked with crosses in Figure 13b. In this interval plasma measurements on the satellite showed that it intersected magnetic field lines connected to the polar arc. The 20-s resolution electric field also shows characteristic variations near the arc, which are smoothed out when averaging over several minutes.

Marklund et al. [1991] found that the relationship between the polar arc and the total convection pattern can change along the arc length depending on the intensity of the convection directly associated with the arc. If a polar arc has low intensity, it can be crossed by convection lines. The resulting total convection is the sum of the quasistationary convection, which exists continuously due to the interaction betwen the solar wind and the Earth's magnetic field, and additional convection in the vicinity of the polar arc. The resulting convection

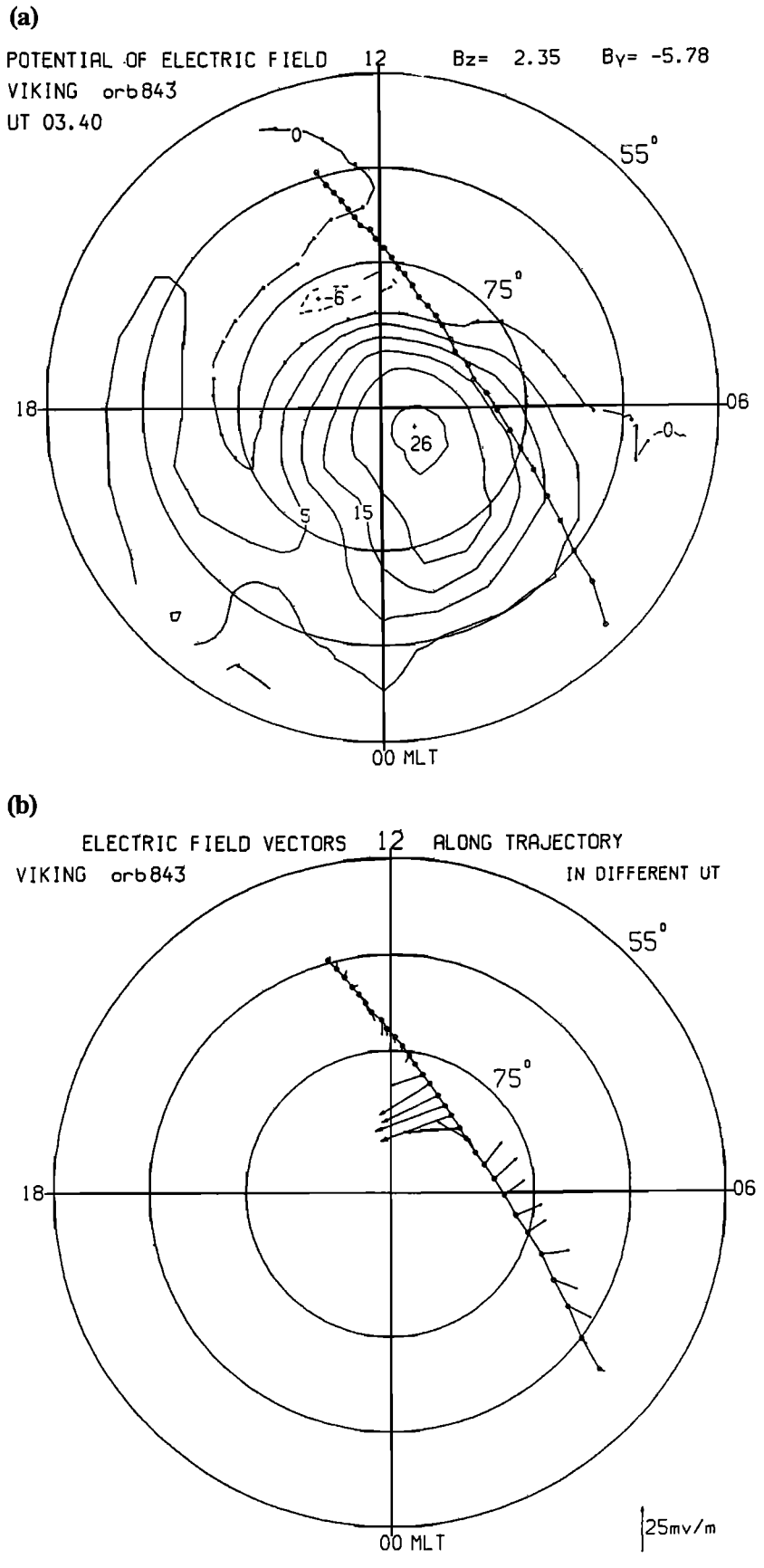

Figure 10. (a) The convection pattern at 0340 UT on July 25, 1986, for IMF components values $B_z = 2.35$ nT and $B_y = -5.78$ nT. The dots along the satellite track correspond to the satellite location every 4 min between 0225 and 0415 UT. (b) The electric field vectors E^m along the satellite track at 4-min intervals using an IMF time shift $\Delta T = 20$ min.

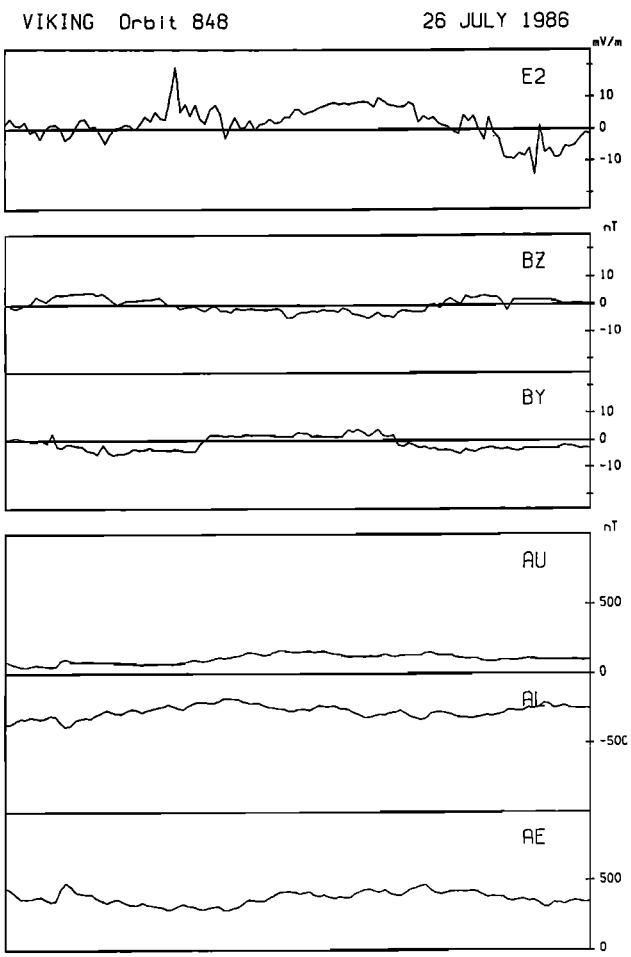

Figure 11. Similar to Figure 2 but for Viking pass 848 over the high-latitude region on July 26, 1986. The IMP 8 spacecraft position is (2.9, 32.8, −3.6) R_E.

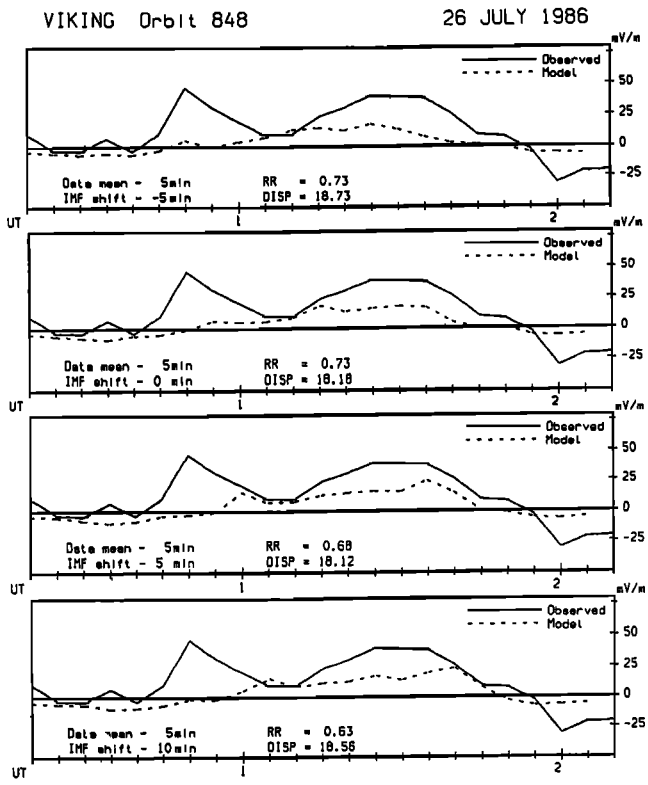

Figure 12. Similar to Figure 8 with a constant averaging time interval of 5 min.

can be directed not along the arc, as is usually assumed, but at an angle to the arc.

In the case studied here, sunward convection is observed everywhere equatorward of the polar arc, and it is possible that the arc is indeed associated with a region of convection reversal. The polar arc is located near the focus of the dawn convection cell (Figure 13b), i.e., in the region of large-scale field-aligned current flowing into the ionosphere. This corresponds to the region 1 currents of *Iijima and Potemra* [1986], but it does not exclude the possibility that there is a small-scale upward field-aligned current immediately above the polar arc. In fact, such a current was detected by the Viking satellite.

Discussion

The establishment of quantitative relations that describe the relation of ionospheric electromagnetic parameters (fields and currents) to the conditions of the solar wind, of which the IMF magnitude and direction are the most important ones, is one of the most acute problems in solar-terrestrial physics. The electric fields in the high-latitude ionosphere, which are determined by the state of the interplanetary medium and the magnetosphere, may be described using models of the large-scale electric fields and currents. Such models, which are based on the method of reconstruction of the large-scale current systems from ground-based magnetic data [*Levitin et al.*, 1984; *Friis-Christensen et al.*, 1985; *Mishin*, 1990] or satellite measurements of electric fields at ionospheric altitudes [*Rich and Maynard*, 1989] are capable of describing the spatio-temporal distribution of the electric field in the high-latitude region (see Figures 4, 7, 12, and 13). The actual capability of the above presented models to predict and reconstruct parameters in the near-Earth space is determined, first of all, by the directness of the connection between the solar wind and the variations in the magnetosphere-ionosphere system. If the processes in the system are directly driven by the solar wind [*Akasofu*, 1979], the models can provide high correlation between the predicted and observed near-space characteristics. If the correlation is low this may imply either unadequacy of the model used or the dominance in the system of "loading-unloading" processes over the directly driven ones. The loading-unloading processes are related to the magnetic energy storage in the magnetospheric tail (loading phase) with its subsequent release, i.e., an "unloading" of the magnetic energy stored in the tail [*McPherron*, 1979; *Baker et al.*, 1984].

The high correlation obtained here between the model and observed electric fields during the growth and expansion phases of magnetospheric substorms suggests

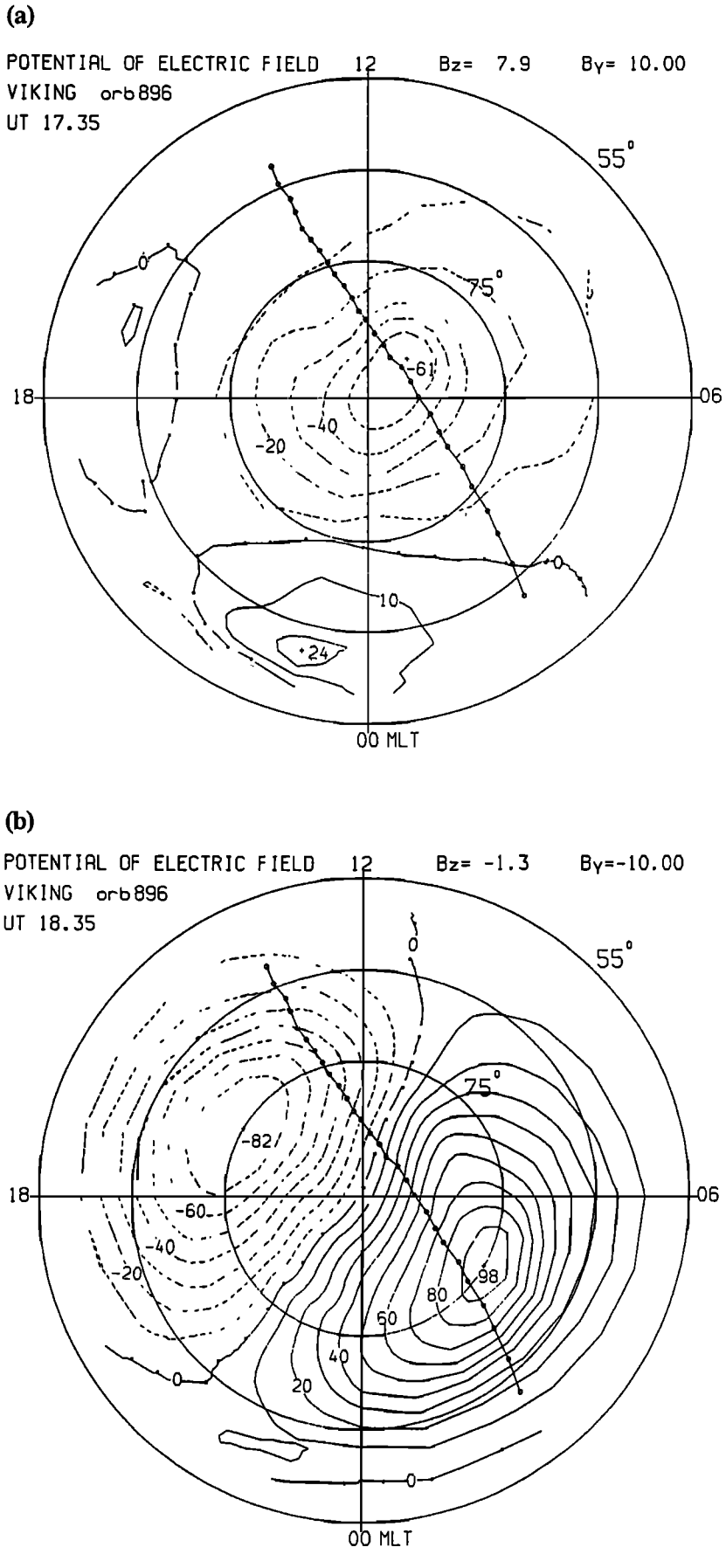

Figure 13. Comparison of E_2 and E_2^m for various values of IMF time shifts ΔT relative to E_2 with a constant averaging time of 5 min.

that the magnetosphere at these times is primarily a driven system and that unloading of magnetotail energy contributes only a minor amount to the observed electric field variations. Processes within the magnetosphere are more prominent during the substorm recovery phase, making the correlation between the model and observed values substantially poorer. It is not excluded that these processes are connected with energy dissipation stored in the magnetospheric tail during the initial phases of the substorm (loading-unloading scenario). The contribution of the intramagnetospheric processes leads to the mitigation of direct connection between the magnetospheric state and the interplanetary medium conditions. Recent results on this topic are contradictory concerning the relation between magnetospheric disturbances and the solar wind electric field (E_{sw}). *Goertz et al.* [1993] found correlation with the auroral zone magnetic disturbances (AE index) at a $\sim$ 90 % level, but *Baker et al.* [1993] found the loading-unloading processes prevailing in generating magnetic disturbances in the westward electrojet region (AL index) [cf. *Akasofu*, 1994]. Such strikingly contradictory results may be explained, at least partially, by differences in the used nonlinear models, but also to some extent by the necessity to discriminate the disturbances under investigation according to the phases of the substorm and a more detailed consideration of time shifts between E_{sw} and the magnetic indices AE and AL.

The optimum time shift $\Delta T = 20$ min shall be compared to the time it takes for IMF variations to propagate to the magnetosphere. The solar wind needs another 4.5 min to reach the magnetopause [*Spreiter and Stahara*, 1980]. According to *Clauer and Banks* [1986] the ionospheric convection responds to IMF variations on the magnetopause with $\sim$ 14-min delay. *Greenwald et al.* [1990] estimate this delay to be 5-9 min, and *Sergeev et al.* [1986] suggest a time delay of 10 min in the response of polar cap convection to discontinuities in the IMF at the bow shock. The time shifts obtained in this study are consistent with these values.

High values of a correlation coefficient indicate a similarity of variation and, hence, the existence of a definite relation between the correlated phenomena. Another

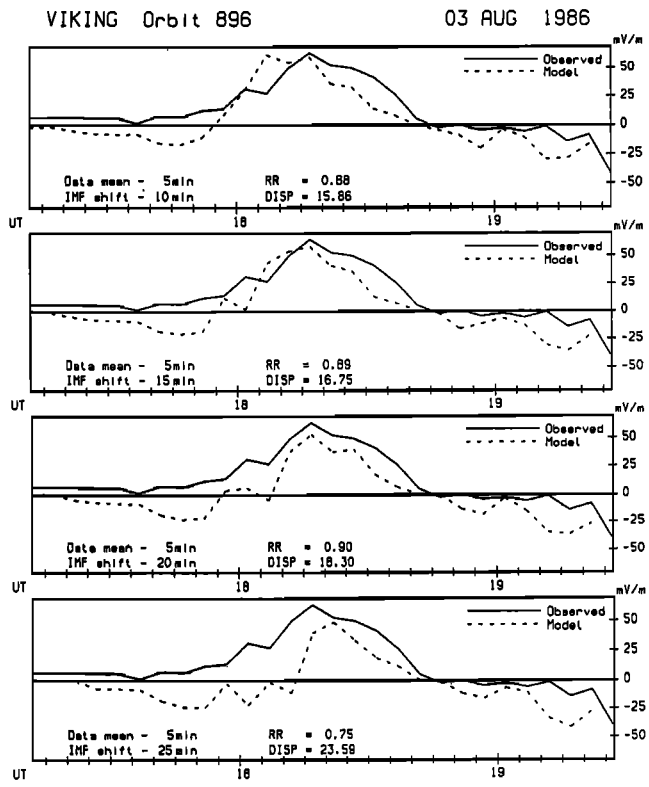

Figure 14. High latitude convection systems of the northern hemisphere during the magnetically quiet interval ($B_z = 10$ nT, $B_y = 6$ nT) (a), and during the growth phase of a substorm ($B_z = -4$ nT, $B_y = -10$ nT) (b) for the Viking pass on August 3, 1986. The polygonal line indicates the ionospheric footpoint (100 km) of the satellite track, the dots correspond to the satellite location every 5 min between 1710 and 1925 UT. Extrema of the potential values are indicated in the foci. The potential difference between isolines is 10 kV; zero equipotential is marked by the dotted line. The two crosses mark the Viking satellite position at 1837 and 1906 UT.

important characteristic of their quantitative relation is the mean square deviation (dispersion) between E_2 and E_2^m. In the course of the growth and expansion phases the dispersion over the whole pass is $\sim$ 15 % of the electric field variation amplitude, and it increases up to $\sim$ 25 % during the recovery phase. A dispersion of 15 % does not exclude the influence of unloading processes on the substorm dynamics during its two first phases.

An important input parameter in the modeling is the ionospheric conductivity distribution. The statistical model by *Wallis and Budzinski* [1981] for $K_p < 3$ and $K_p > 3$ which has been used here in the model calculations to represent IMF $B_z \geq 0$ and IMF $B_z < 0$ conditions, respectively, provides, of course, only a crude approximation of the actual conditions prevailing during the Viking passes. In particular, during pass 896 it does not take into account conductivity enhancements associated with the θ aurora inside the polar cap. It is known, that the distribution of the electrostatic potential and the electric field is critically dependent on the ionospheric conductivity [cf. *Blomberg and Marklund*, 1988; *Ahn et al.*, 1989]. However, during the summer season the electromagnetic radiation component of the height-integrated ionospheric conductivity exerts a stabilizing effect on the resultant conductivity distribution. Its existence smooths out conductivity irregularities associated with particle precipitation. Apparently, the increase in the component of the conductivity due to particle precipitation does not crucially influence the large-scale features of the electrostatic potential and electric field distributions during summer.

When modeling the convection and electric field during the Viking passes, it was necessary to take into account the variations in the interplanetary medium. During the time interval of about 2 hours it took the Viking satellite to cross the high-latitude region drastic changes of the IMF orientation and intensity took place. Modeling of the whole pass using only one representative state of the magnetosphere is therefore not adequate. For instance, Viking pass 896 on August 3, 1986, corresponds to an interval for which a transpolar luminosity band (θ aurora) existed in the polar cap. *Burch et al.* [1992] used a northward IMF merging model containing lobe cells, merging cells, and viscous cells to interpret the large-scale convection for such an event. It was assumed that the magnitudes of the IMF components can be obtained as mean values over a reasonably long time span to characterize the IMF conditions during the event. If such a procedure is used for the August 3, 1986, event the average value of the IMF B_z component over the time interval from 1 hour before the auroral observation until the end of observations (1700-1926 UT) becomes $B_z = 6.6$ nT. All other cases considered by *Burch et al.* [1992] were characterized by a northward IMF direction. Therefore one may be led to conclude that θ aurora events are characterized exclusively by sunward convection in the central polar cap. The event on August 3, 1986, does not fit this conventional scheme. It appeared that during the life time of the θ aurora drastic changes of the large-scale convection occurred. In particular, during the $B_z < 0$ interval the convection across the central part of the polar cap is antisunward. Therefore, during times of θ aurora the convection via the central part of the polar cap is frequently sunward, but in other time intervals the convection direction may become antisunward. This fact must be taken into account when constructing models of θ auroras.

Another event similar to the August 3, 1986, treated here with $B_z > 0$ initially followed by a southward turning of the IMF was Viking pass 1188 on September 25, 1986, analyzed in detail by *Marklund et al.* [1991].

Summary

The IZMEM model for reconstructing the electric fields and horizontal currents in the high-latitude ionosphere was applied to five events occurring during different phases of magnetospheric substorms. The results were compared to in situ Viking electric field data. The level of agreement between the measured and the modeled electric field is different during different phases. This leads us to the following conclusions.

The IZMEM model, and also other similar models relating the electrodynamics of the high-latitude ionosphere to the interplanetary medium, are a useful tool for describing the system. The high correlation between model and observations for growth and expansion phase is suggests that at these times the magnetosphere is mainly directly driven by the solar wind. During recovery phase processes internal to the magnetosphere, i.e., loading-unloading are more prominent, and therefore there is a poorer correlation between model and observations.

In the modeling it is necessary to account for the finite transit time from the solar-wind spacecraft to the magnetopause and also for the intramagnetospheric time delay. The optimum time delays found in this study are consistent with typical delay times discussed in the literature. Another necessity was to account for changes in the IMF during the course of Viking's traversal of the high-latitude region.

Acknowledgments. The Viking Project was managed and operated by the Swedish Space Corporation under contract from the Swedish Board for Space Activities. This work was supported by the Russian Foundation of Fundamental Researches (project codes 93-05-8722 and 94-05-16350), grant N M6P000 from the International Science Foundation, and by the Swedish National Space Board.

The Editor thanks Roderick A. Heelis and another referee for their assistance in evaluating this paper.

References

Ahn, B.-H., Y. Kamide, S.-I. Akasofu, H. W. Kroehl, D. J. Gorney, Ionospheric conductivity dependence of the cross polar cap potential difference and global Joule heating rate, *J. Atmos. Terr. Phys., 51,* 841-859, 1989.

Akasofu, S.-I., Interplanetary energy flux associated with magnetospheric substorms, *Planet. Space Sci., 27,* 425-431, 1979.

Akasofu, S.-I., Energy coupling between the solar wind and the magnetosphere, *Space Sci. Rev., 28*, 121-190, 1981.

Akasofu, S.-I., Assessing the magnetic reconnection paradigm, *Eos Trans. AGU, 75*, 249, 1994.

Baker, D. N., S.-I. Akasofu, W. Baumjohann, J. W. Bieber, D. M. Fairfield, E. W. Hones, B. Mauk, R. L. McPherron, and T. E. Moor, Substorms in the magnetosphere, in *Solar-Terrestrial Physics: Present and Future*, edited by D. M. Butler and K. Paradopoulos, *NASA Ref. Publ., 1120*, 8-3, 1984.

Baker, D. N., T. A Fritz, R. L. McPherron, D. H. Fairfield, Y. Kamide, and W. Baumjohann, Magnetotail energy storage and release during the CDAW6 substorm analysis interval, *J. Geophys. Res., 90*, 1205-1216, 1985.

Baker, D. N. A. J. Klimas, T. I. Pulkkinen, and R. L. McPherron, Re-examination of driven and unloading aspects of magnetospheric substorms, *Adv. Space Res., 13(4)*, 75-83, 1993.

Bilitza, D., Solar-terrestrial models and application software, *90-19*, 18, Nat. Space Sci. Data Cent., World Data Cent. A for Rockets and Satellites, Greenbelt, Md., 1990.

Block, L. P., C.-G. Falthammar, P.-A. Lindqvist, G. T. Marklund, F. S. Mozer, and A. Pedersen, Measurement of quasistatic and low frequency electric fields on the Viking satellite, *Rep. TRITA-EPP-87-02*, Royal Inst. Tech., Stockholm, 1987.

Blomberg, L. G., and G. T. Marklund, The influence of conductivities consistent with field-aligned currents on high-latitude convection patterns, *J. Geophys. Res., 93*, 14,493-14,499, 1988.

Blomberg, L. G. and G. T. Marklund, High-latitude electrodynamics and aurorae during northward IMF, in *Auroral Plasma Dynamics*, Geophys. Monogr. vol. 80, edited by R. Lysak, pp. 55-68, AGU, Washington, D. C., 1993.

Burch, J. L., P. H. Reiff, J. D. Menietti, R. A. Heelis, W. B. Hanson, S. D. Shawhan, E. G. Shelley, M. Sugiura, D. R. Weimer, and J. D. Winningham, IMF B_y-dependent plasma flow and Birkeland currents in the dayside magnetosphere, 1, Dynamics Explorer observations, *J. Geophys. Res., 90*, 1577-1594, 1985.

Burch, J. L., N. A. Saflekos, D. A. Gurnett, J. D. Craven, L. A. Frank, The quiet time polar cap: DE-1 observations and conceptual model, *J. Geophys. Res., 97*, 19,403-19,412, 1992.

Clauer, C. R., and P. M. Banks, Relationship of the interplanetary electric field to the high-latitude ionospheric electric fields and currents: Observations and model stimulation, *J. Geophys. Res., 91*, 6959-6971, 1986.

Cogger, L. L., and J. S. Murphree, The UV auroral distribution: Its impulsive nature, *Adv. Space Res., 10(6)*, 167-177, 1990.

Craven, J. D., and L. A. Frank, Diagnosis of auroral dynamics using global auroral imaging with itasis on large-scale evolution, in *Auroral Physics*, edited by C.-I. Meng, M. J. Rycroft, and L. A. Frank, pp. 273-288, Cambridge Univ. Press, New York, 1991.

Craven, J. D., J. S. Murphree, L. A. Frank, and L. L. Cogger, Simultaneous optical observations of transpolar arcs in the two polar caps, *Geophys. Res. Lett., 18*, 2297-2300, 1991.

Dremuhina, L. A., A. E. Levitin, and Y. I. Feldstein, Convection in high-latitudes during intervals with $B_z > 0$, *Geomagn. Aeron., 30*, 190-194, 1990.

Faermark, D. S., A restoration of 3-dimensional current system in high-latitudes by the use of ground-based geomagnetic observations, *Geomagn. Aeron., 17*, 163-165, 1977.

Feldstein, Y. I., Night-time aurora and its relation to the magnetosphere, *Ann. Geophys., 30*, 259-272, 1974.

Feldstein, Y. I., and A. E. Levitin, Solar wind control of electric fields and currents in the ionosphere, *J. Geomagn. Geoelectr., 38*, 1143-1182, 1986.

Feldstein, Y. I., A. E. Levitin, D. S. Faermark, R. G. Afonina, B. A. Belov, V. Y. Gaidukov, Electric field and potential patterns in the high-latitude ionosphere for different situation in interplanetary space, *Planet. Space Sci., 32*, 907-923, 1984.

Feldstein, Y. I., G. V. Vorobjev, R. D. Elphinstone, and I. I. Alexeev, Auroras in the polar cap, *IRF Sci. Rep. 209*, 123-140, 1992.

Feldstein, Y. I., A. E. Levitin, L. I. Gromova, G. T. Marklund, L. G. Blomberg, and P.-A. Lindqvist, Electromagnetic Weather over the High-Latitude Ionosphere During the Aurora in the Polar Cap, *Cosmic Research, 33*, 326-335, 1995.

Frank, L. A., et al. The theta aurora, *J. Geophys. Res., 91*, 3177-3224, 1986.

Friis-Christensen, E., Y. Kamide, A. D. Richmond, and S. Matsushita, Interplanetary magnetic field control of high-latitude electric fields and currents determined from Greenland magnetometer data, *J. Geophys. Res., 90*, 1325-1338, 1985.

Goertz, C. K., L.-H. Shan, and R. A. Smith, Prediction of geomagnetic activity, *J. Geophys. Res., 98*, 7673-7684, 1993.

Greenwald, R. A., K. B. Baker, J. M. Ruohoniemi, J. R. Dudeney, M. Pinnock, N. Mattin, J. M. Leonard, and R. P. Lepping, Simultaneous conjugate observations of dynamic variations on high-latitude dayside convection due to changes on IMF B_y, *J. Geophys. Res., 95*, 8057-8072, 1990.

Gusev, M. G., and O. A. Troshichev, Relation of Sun-aligned arcs to polar cap convection and magnetic disturbances, *Planet. Space Sci., 39*, 1-11, 1990.

Hoffman, R. A., R. A. Heelis, and J. S. Prasad, A Sun-aligned arc observed by DMSP and AE-C, *J. Geophys. Res., 90*, 9697-9710, 1985.

Iijima, T., and T. A. Potemra, The amplitude distribution of field-aligned currents at northern high latitudes observed by Triad, *J. Geophys. Res., 81*, 5971-5979, 1976.

Kamei, T., M. Sugiura, and T. Araki, *Data Book N20*, World Data Cent. C2 for Geomagnetism, Kyoto, Japan, 1991.

Kamide, Y., A. D. Richmond, and S. Matsushida, Estimation of ionospheric electric fields, ionospheric currents and field-aligned currents from ground magnetic records, *J. Geophys. Res., 86*, 801-813, 1981.

Levitin, A. E., R. G. Afonina, B. A. Belov, and Y. I. Feldstein, Geomagnetic variation and field-aligned currents at northern high-latitudes and their relations to solar wind parameters, *Philos. Trans. R. Soc. London Ser. A, 304*, 253-301, 1982.

Levitin, A. E., Y. I. Feldstein, R. G. Afonina, B. A. Belov, L. A. Dremuhina, D. S. Faermark, Y. Z. Demidova, M. Y. Markova, S. I. Avdushin, and V. Y. Gaiducov, The model large-scale electric field and currents in high-latitude ionosphere, parts 1-6, Gidrometeoizdat, Moscow, 1984.

Lindqvist, P.-A., G. T. Marklund, A statistical study of high-latitude electric fields measured on the Viking satellite, *J. Geophys. Res., 95*, 5867-5876, 1990.

Lotko, W., Milestones in Geospace Environment Modeling, *Eos Trans AGU, 74*, 618-622, 1993.

Marklund, G. T., and L. G. Blomberg, Toward a better understanding of the global auroral electrodynamics through numerical modeling studies, in *Magnetospheric Substorms*, Geophys. Monogr. Ser., vol. 64, edited by J. R. Kan et al., pp. 305-319, AGU, Washington, D. C., 1991.

Marklund, G. T., L. G. Blomberg, K. Stasiewicz, J. S. Murphree, R. Pottelette, L. J. Zanetti, T. A. Potemra, D. A. Hardy, and F. J. Rich, Snapshots of high-latitude electrodynamics using Viking and DMSP F7 observations, *J. Geophys. Res., 93*, 14,479-14,492, 1988.

Marklund, G. T., L. G. Blomberg, J. S. Murphree, R. D. Elphinstone, L. J. Zanetti, R. E. Erlandson, I. Sandahl, O. de la Beaujardiere, H. Opgenoorth, and F. J. Rich, On the electrodynamical state of the auroral ionosphere during northward interplanetary magnetic field: A transpolar arc case study, *J. Geophys. Res., 96,* 9567-9578, 1991.

McPherron, R. L. Growth phase of magnetospheric substorms, *J. Geophys. Res., 75,* 5592-5599, 1970.

McPherron, R. L., Magnetospheric substorms, *Rev. Geophys., 17,* 657-681, 1979.

Mishin, V. M., The magnetogram inversion technique and some applications, *Space Sci. Rev., 53,* 83-163, 1990.

Murphree, J. S., J. B. Austin, D. J. Hearn, L. L. Cogger, and R. D. Elphinstone, Satellite observations of polar arc, *J. Atmos. Terr. Phys., 56,* 265-284, 1994.

Papitashvili, V. O., B. A. Belov, D. S. Faermark, Y. I. Feldstein, S. A. Golyshev, L. I. Gromova, and A. E. Levitin, Electric potential patterns in the northern and southern polar regions parametrized by the interplanetary magnetic field, *J. Geophys. Res., 99,* 13,251-13,262, 1994.

Reiff, P. H., and J. L. Burch, IMF B_y-dependent plasma flow and Birkeland currents in the dayside magnetosphere, 2, A global model for northward and southward IMF, *J. Geophys. Res., 90,* 1595-1609, 1985.

Reiff, P. H., and J. G. Luhmann, Solar wind control of the polar cap voltage, in *Solar Wind-Magnetosphere Coupling,* edited by Y. Kamide and J. A. Slavin, 453-476, Terra, Tokyo, 1986.

Rich, F. J., and N. C. Maynard, Consequences of using simple analytical functions for the high-latitude convection electric field, *J. Geophys. Res., 94,* 3687-3701, 1989.

Richmond, A. D., Assimilative mapping of ionospheric electrodynamics, *Adv. Space Res., 12,* 59-65, 1992.

Richmond, A. D., and Y. Kamide, Mapping electrodynamical features of the high-latitude ionosphere from localized observations: Technique, *J. Geophys. Res., 93,* 5741-5759, 1988.

Richmond, A. D., et al., Mapping electrodynamic features of the high-latitude ionosphere from localized observations: Combined incoherent-scatter radar and magnetometer measurements for January 18-19, 1984, *J. Geophys. Res., 93,* 5760-5776, 1988.

Robinson, R. M., and R. R. Vondrak, Measurement of E region ionization and conductivity produced by solar illumination at high latitudes, *J. Geophys. Res., 89,* 3951-3956, 1984.

Sergeev, V. A., N. P. Dmitrieva, and E. S. Barkova, Triggering of substorm expansion by the IMF directional discontinuities: Time delay analysis, *Planet. Space Sci., 34,* 1109-1118, 1986.

Spreiter, J. R., and S. S. Stahara, A new predictive model for determining solar wind-terrestrial planet interaction, *J. Geophys. Res., 85,* 6769-6777, 1980.

Vorobjev, V. G., S. V. Leontiev, and Y. I. Feldstein, Extended period of polar cap auroral display: Auroral dynamics and relation to the IMF and ionospheric convection, *Ann. Geophys., 13,* 854-862, 1995.

Wallis, D. D., and E. E. Budzinski, Empirical models of height integrated conductivities, *J. Geophys. Res., 86,* 125-137, 1981.

Weber, E. J., et al., Rocket measurements within a polar cap arc: Plasma, particle, and electric circuit parameters, *J. Geophys. Res., 94,* 6692-6712, 1989.

L. G. Blomberg, P.-A. Lindqvist, and G. T. Marklund, Alfvén Laboratory, Royal Institute of Technology, S-100 44 Stockholm, Sweden.

Y. I. Feldstein, L. I. Gromova, and A. E. Levitin, IZMIRAN, 142092 Troitsk, Moscow Region, Russia.

(Received June 15, 1993; revised November 10, 1995; accepted February 1, 1996.)